Atomically Resolved Images from Near Node Photoelectron Holography Experiments on Al(111)

J. Wider,[1] F. Baumberger,[1] M. Sambi,[2] R. Gotter,[3] A. Verdini,[3] F. Bruno,[3,4] D. Cvetko,[5,6] A. Morgante,[3,4] T. Greber,[1,*] and J. Osterwalder[1]

[1]*Physik Institut der Universität Zürich, Winterthurerstrasse 190, CH-8057 Zürich, Switzerland*
[2]*Università di Padova, Dipartimento di Chimica Inorganica, Metallorganica ed Analitica, Via Loredan 4, I-35131 Padova, Italy*
[3]*Laboratorio TASC, Istituto Nazionale per la Fisica della Materia, Basovizza SS14 Km 163.5, I-34012 Trieste, Italy*
[4]*Department of Physics, University of Trieste, Via Valerio 2, I-34100 Trieste, Italy*
[5]*Sincrotrone Trieste SCpA, Basovizza SS14 Km 163.5, I-34012 Trieste, Italy*
[6]*Jožef Stefan Institute, Department of Physics, Ljubljana University, Ljubljana, Slovenia*
(Received 15 September 2000)

Szöke's concept for electron holography is hampered by forward scattering that dominates electron diffraction from electron point sources below the surface top layer. Forward scattering was proposed to be suppressed if the anisotropic nature of the electron source wave is exploited [T. Greber and J. Osterwalder, Chem. Phys. Lett. **256**, 653 (1996)]. Experiments show a strong suppression of forward scattering in Al(111) if Al 2*s* photoelectrons ($E_{\mathrm{kin}} = 952$ eV) are measured near the nodal plane of the outgoing *p* wave. The holographic reconstruction from such diffraction data provides three dimensional images of atomic sites in unit cells with a size of more than 10 Å.

DOI: 10.1103/PhysRevLett.86.2337 PACS numbers: 61.14.–x, 42.40.–i, 68.35.Bs, 79.60.–i

Far field microscopes are, apart from their obvious advantages, diffraction limited where the resolution scales with the wavelength of the probe. In order to get atomic resolution the wavelength of the probing beam has to be below 1 Å, i.e., photons with more than 10 keV or electrons with more than 150 eV have to be used and accurate lenses have to be at hand. In diffraction experiments no lenses are needed but the information translates not directly in three dimensional images since the phase information of the diffracted beam is lost. Gabor's idea of holography is a way of recovering the phase information and gives access to the full three dimensional structure [1]. Szöke extended holography to x-ray and electron diffraction experiments. His "inside source" concept proposes the x rays or electrons that are created at atomic sites to form a hologram in Gabor's sense [2]. After the emission process the "coherent beam" splits in an unscattered reference wave Ψ_r and a scattered object wave Ψ_o that interfere in the detector.

The measured intensity $\mathrm{I}(\mathbf{k})$ can thus be written as

$$\begin{aligned}\mathrm{I}(\mathbf{k}) &= |\Psi_r + \Psi_o|^2 \\ &= \Psi_r\Psi_r^\star + \Psi_r\Psi_o^\star + \Psi_o\Psi_r^\star + \Psi_o\Psi_o^\star, \quad (1)\end{aligned}$$

where $\mathbf{k}$ is the wave vector of the reference and the object wave. The intensities of a large set of $\mathbf{k}$ vectors constitute a hologram and permit the reconstruction of an image $\mathrm{U}(\mathbf{r})$ in real space. If $\Psi_r\Psi_r^\star$ is known and the object self-interference term $\Psi_o\Psi_o^\star$ is small, $\mathrm{U}(\mathbf{r})$ is determined by the Fourier transform of $\mathrm{I}(\mathbf{k})$, i.e., from the interference terms $\Psi_r\Psi_o^\star + \Psi_o\Psi_r^\star$. These interference terms contain an image and a twin image and there are ways to distinguish the two [3].

For three dimensional images the $\mathbf{k}$ space sample has to span three dimensions. This is achieved in scanning two emission angles and/or the scanning of $|\mathbf{k}|$ (multiple energy sampling) where a uniform sampling gives the best results [4].

Recently, inside source holography with x rays was demonstrated [5]. This kind of holography applies for heavy elements as scatterers and emitters and the probed volume is fairly large. Inside source holography with electrons is more sensitive, in particular to light elements, though several problems are encountered. In the relevant electron kinetic energy range the scattering cross section of electrons is in the order of 1 Å^2 and highly anisotropic. Therefore, multiple scattering is important and the scattering amplitudes and phase shifts are not isotropic. The application of Fourier transforms to recover the real space structure from the diffraction patterns of photoelectron or Auger electron diffraction data is thus not straightforward. Holography with electrons was, however, demonstrated for top layer atoms as electron sources, where the anisotropic scattering is minimal due to the backscattering geometry [6]. In more general geometries photoelectron holography has to put up with forward scattering effects [7]. Forward scattering is a zero order diffraction feature and contains no holographic information. By introducing suitable integration kernels in the Fourier transforms the destructive effects of forward scattering and of scattering phase shifts could be removed in some cases [8], but in other cases this procedure introduces strong artifacts [9,10]. Moreover, in multiple element samples one has to know which scattering phase shifts to use near a particular image site. Thus electron holography lost the charm of predicting a structure without an *a posteriori* input of information such as a distinction between forward scattering and interference patterns from higher order diffraction.

Forward scattering was proposed to be suppressed if the anisotropic nature of the electron source wave is exploited

[11] (see Fig. 1). In a single scattering picture the photoelectron diffraction intensity $I(\mathbf{k})$ [Eq. (1)] may be written as

$$I(\mathbf{k}) = \left| \Psi_{\text{source}}(\vartheta \equiv 0, \mathbf{R}) + \sum_i \frac{f(\vartheta_i)}{|\mathbf{R} - \mathbf{r}_i|} \Psi_{\text{source}}(\vartheta_i, \mathbf{r}_i) \right|^2, \quad (2)$$

where the emitter (source) sits at the origin, $\mathbf{R}$ is the location of the detector, and $\mathbf{r}_i$ the location of the scatterer (object) i. $f(\vartheta_i)$ is the complex scattering amplitude where ϑ_i is the angle between $\mathbf{r}_i$ and $\mathbf{R}$. $\Psi_{\text{source}}(\vartheta \equiv 0, \mathbf{R})$ is the reference wave Ψ_r. It can be seen that the importance of forward scattering $\vartheta_i = 0$ scales with the intensity of the reference wave. Therefore the Fraunhofer condition $|\Psi_r| \gg |\Psi_o|$ can generally not be optimized in electron holography since it would cause strong forward scattering. If the source wave is isotropic the relative weight of the forward scattering is constant. For anisotropic source waves, such as a p wave that is created by the photoexcitation of an s level, the relative importance of the reference wave and thus the weight of forward scattering can be tuned. If, e.g., the electron emission direction lies on a node of the photoemission source wave, no forward scattering is expected. However, within the single scattering picture, such photoelectron diffraction patterns cannot be considered as holograms since the reference wave is missing in this geometry. For 1 keV electrons it was shown by scattering calculations that there is an optimum angle of about 10° near the nodal plane of an outgoing p wave, where the holographic reconstructions are best [11]. This angle is a compromise between the weight of the disturbing object self-interference term $\Psi_o \Psi_o^\star$ and that of the forward scattering. In Fig. 1 the *far node* geometry is compared with the *near node* geometry. It is seen that in the near node geometry the relative weight of the interference pattern is strongly enhanced compared to the forward scattering. It has to be noted that near node photoelectron holography requires a constant angle γ between the detector and the light polarization. Otherwise, the near node condition is not fulfilled for all emission directions. Therefore, in this kind of experiment, the sample has to be rotated with respect to the reference frame of the light source and the detector. This has the further advantage that the contribution of the reference wave to the diffraction intensity is constant. In this Letter the first experimental confirmation of highly improved holographic images from near node photoelectron diffraction data is reported. In a multilayer object like an Al(111) crystal forward scattering is a strong contribution in standard photoelectron diffraction data. It is shown that the suppression of forward scattering leads to atomically resolved images of atomic sites and that not even the multiple energy approach [12] has to be involved.

The experiments have been performed at the ALOISA beam line at the synchrotron facility ELETTRA [13]. Atomically clean Al(111) surfaces have been prepared

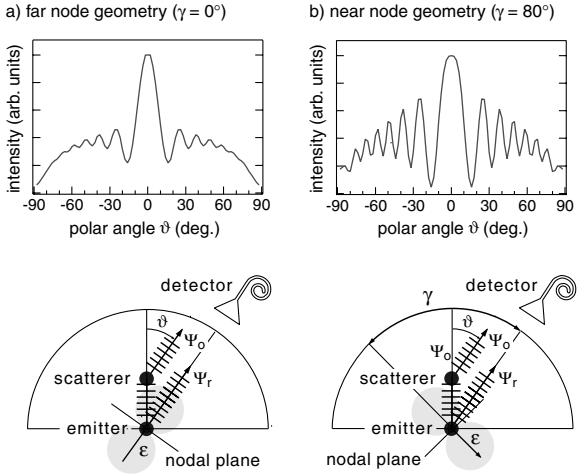

FIG. 1. Principle of photoelectron holography and near node photoelectron holography illustrated for an aluminum dimer. The scattered wave Ψ_o and the unscattered wave Ψ_r interfere in the detector and form, if measured at many different angles ϑ, a hologram. The holograms are simulated with single scattering calculations: The Al 2s emitter (inside source) is 2.86 Å away from the Al scatterer (object) and produces a p wave with a wavelength of 0.4 Å. The situations for two different orientations γ of the light polarization $\boldsymbol{\varepsilon}$ relative to the electron detector are shown. These angles γ remain fixed during the recording of the hologram. In the far node geometry ($\gamma = 0°$), (a), the diffraction is dominated by the forward scattering at $\vartheta = 0°$. In the near node geometry, (b), where the angle γ is nearly 90°, the higher order interference fringes at $\vartheta \neq 0°$ are strongly enhanced, relative to the forward scattering.

using standard techniques. The face centered cubic (fcc) structure with a nearest neighbor distance of 2.86 Å is well known and no surface reconstruction occurs. Furthermore, the inversion symmetry of the fcc structure causes the twin images to coincide with the image. The experiments were performed at room temperature. The Al 2s diffraction data sets contain about 1600 data points evenly spaced in $2\pi/3$ from normal emission down to a polar angle of 70°. With the photon energy of 1070 eV and the binding energy of the Al 2s core level (118 eV), the electron wavelength becomes 0.4 Å. Two orientations of the linear light polarization were used. The horizontal polarization vector, the surface normal, and the direction of detection lie in a single plane. In the *near node* geometry the angle γ between the detector and the polarization was set to 80° and in the *far node* geometry to 0°. The far node geometry data serve for comparison, the absolute determination of the crystal orientation and the compensation of the residual vertical polarization component that was determined to be about 5%. The subtraction of the photoemission intensity of the vertical polarization is allowed since the horizontal and vertical polarization components contribute incoherently. In order to remove the polar angle dependence of the instrumental response function, the azimuthal data sets [Figs. 2(a) and 2(c)] are normalized for every polar emission angle.

This normalization procedure decreases the holographic sensitivity in the vertical direction. This is no major problem for the present case of Al(111) since in this direction the nearest atoms are 7 Å away from the emitter.

Figure 2 demonstrates near node photoelectron diffraction (and holography) with experimental data. The angular Al 2*s* photoemission intensities for the far node and the near node geometry are stereographically projected in Figs 2(a) and 2(c). White corresponds to highest and black to lowest intensity. From comparison with Fig. 2(b) which shows the corresponding real space projection of a fcc crystal on the (111) plane it is seen that the far node diffraction pattern can be regarded as a projection of nuclear charge along the nearest neighbor directions. The forward scattering focuses intensity along nearest neighbors and thus causes high intensity along low index atomic chains and planes [7]. This correspondence is not seen in the near node diffraction pattern [Fig. 2(c)] and thus indicates suppression of forward scattering. In order to get real space images of the emitter's environment the diffraction patterns are holographically interpreted by the Stuck algorithm [14]. Care was taken by considering an apodizing function that smoothes the edges of the diffraction patterns. This avoids unwanted high frequency components, i.e., artifacts in the Fourier transform. The image function $|\mathbf{r}U(\mathbf{r})|^2$ is shown after a convolution with a Gaussian with 1 Å full width at half maximum without any low intensity cutoff. The convolution averages out the rapid $\sin(\mathbf{kr})$ oscillations in $U(\mathbf{r})$ [14]. In the near node geometry the holographic reconstruction of real space around the emitter in the (111) plane clearly reveals the positions of the surrounding atoms. In Figure 2(f) nearest, next nearest, and even second next nearest neighbor positions are resolved as local maxima in the image. This is not the case for the far node geometry data where no distinct atomic positions but a "nearest neighbor belt" is found. As usual in inside

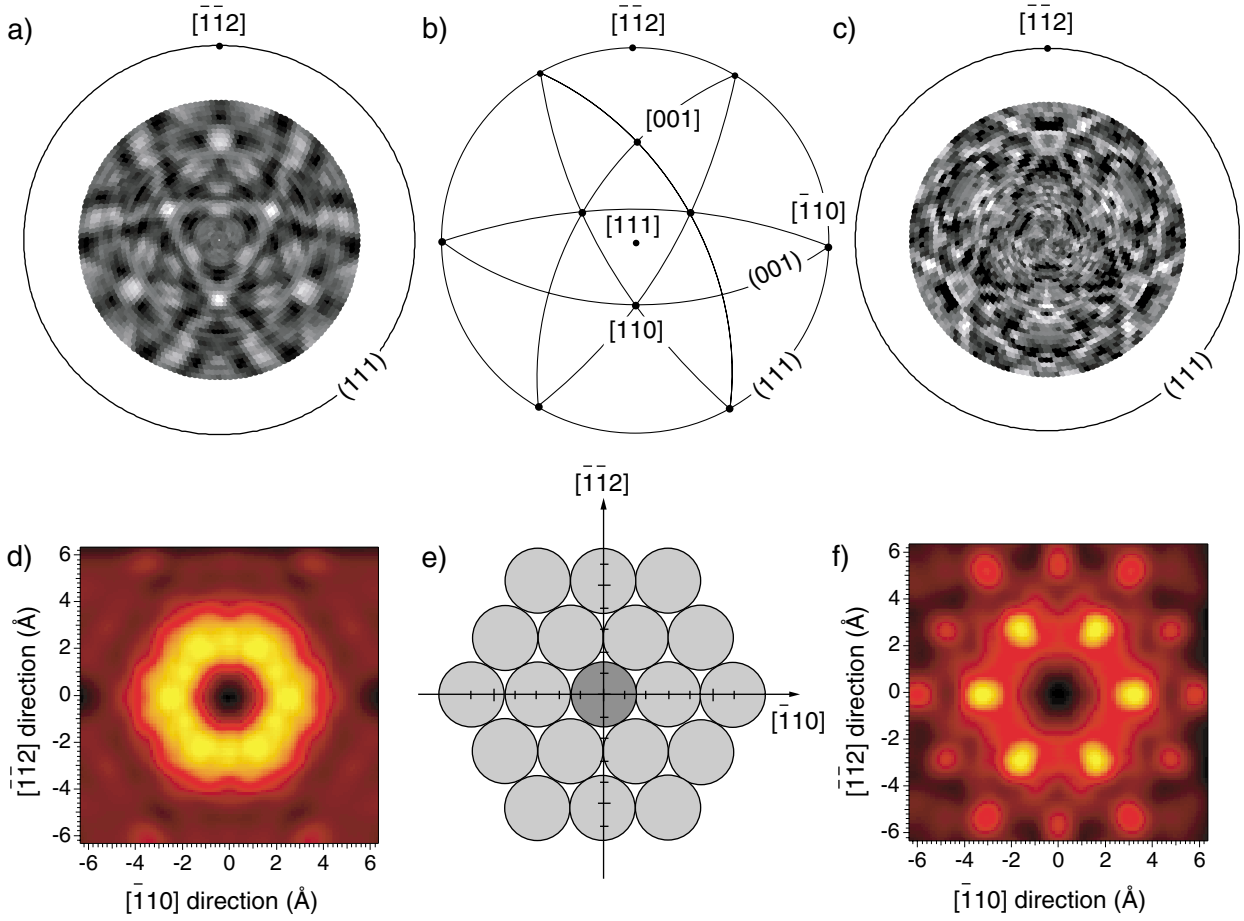

FIG. 2 (color). Comparison of far node and near node photoelectron diffraction data and their holographic reconstructions. (a) and (c): Stereographically projected experimental Al 2*s* ($E_{\text{kin}} = 952$ eV) photoelectron diffraction patterns from an Al(111) single crystal for the far node and the near node geometry. In the far node geometry (a) forward scattering dominates the pattern as can be seen from the stereographic projection of the high density crystal chains and planes in (b). In the near node diffraction pattern (hologram) no distinct forward scattering features are visible. (d) and (f): Corresponding holographic real space reconstructions of a plane parallel to the surface that contains the emitter (inside source) at (0, 0). They should show the expected image of an Al(111) plane (e). In the near node reconstruction (f) nearest, next nearest, and second next nearest neighbors are clearly resolved as local maxima while in the far node picture (d) no clear atom positions can be seen.

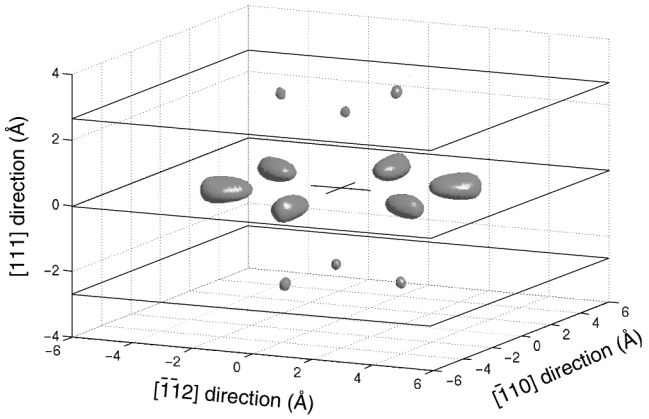

FIG. 3. Three dimensional isointensity representation of the holographic image as reconstructed from the photoelectron diffraction data in Fig. 2(c). The atomic environment of an Al $2s$ photoemitter at $(0, 0, 0)$ in Al(111) is shown inside a shell with 4 Å radius.

source holography, the emitter sits at the origin of the image and is not reproduced.

In Fig. 3 a three-dimensional image of the holographic reconstruction of the data in Fig. 2(c) is displayed. The convoluted image function is shown within a sphere around the emitter with 8 Å diameter. Intensities greater than 83% of the maximum intensity are displayed opaque. The image is remarkably free of noise. The image quality in the [111] direction, normal to the surface, is not as good as in the (111) plane. This can be partly understood in considering that the emitters in the top layers do see truncated neighbor shells and that the thermal smearing is more pronounced normal to the surface. Furthermore, the $k_{[111]}$ sampling is more limited in our experimental setup. The photoelectrons were recorded down to emission angles of 70° only and diffraction intensity modulations in the [111] direction have been averaged out because the instrumental transmission function along the polar angle is difficult to determine. This can be improved in experiments where the intensity modulations along the polar angle are measured over the whole emission hemisphere. However, from the data in Fig. 2(c) the three dimensional structure of the twelve nearest neighbors around the emitter is recovered. In Fig. 3 the expected ABC stacking of subsequent (111) planes in the fcc structure is correctly reproduced. The atoms in the (111) planes below and above the emitter appear with lower intensities and the holographic image is not very precise with respect to the *absolute* length. This is caused by the atomic scattering phase shifts that imply larger and anisotropic "effective" scattering paths. All nearest neighbor distances in Fig. 3 are overestimated by about one wavelength, but in a fairly isotropic way. The twelve emitter-nearest neighbor distances scatter by 0.1 Å around the mean value of 3.4 Å (instead of 2.86 Å as expected from the fcc structure of aluminum).

These findings demonstrate that the atomic structure of molecular objects with a size in the order of 10 Å can be explored with near node photoelectron holography, even at the single energy level. It is a method for direct structure determination and will supplement standard trial and error methods.

It is a pleasure to acknowledge the Instituto Nazionale per la Fisica della Materia (INFM) for beam time and hospitality and the Swiss National Science Foundation who supports this project.

*Corresponding author.
Email address: greber@physik.unizh.ch

[1] D. Gabor, Nature (London) **161**, 777 (1948).
[2] A. Szöke, in *Short Wavelength Coherent Radiation: Generation and Applications,* edited by D. T. Attwood and J. Boker, AIP Conf. Proc. No. 147 (AIP, New York, 1986), pp. 361–467.
[3] J. J. Barton, Phys. Rev. Lett. **67**, 3106 (1991).
[4] P. M. Len, S. Thevuthasan, A. P. Kaduwela, M. A. Van Hove, and C. S. Fadley, Surf. Sci. **365**, 535 (1996).
[5] M. Tegze, G. Faigel, S. Marchesini, M. Belakhovsky, and A. I. Chumakov, Phys. Rev. Lett. **82**, 4847 (1999).
[6] H. Wu, G. J. Lapeyre, H. Huang, and S. Y. Tong, Phys. Rev. Lett. **71**, 251 (1993).
[7] C. S. Fadley, Surf. Sci. Rep. **19**, 231 (1993).
[8] B. P. Tonner, Z.-L. Han, G. R. Harp, and D. K. Saldin, Phys. Rev. B **43**, 14 423 (1991).
[9] A. Stuck, D. Naumović, T. Greber, J. Osterwalder, and L. Schlapbach, Surf. Sci. **274**, 441 (1992).
[10] J. Osterwalder, R. Fasel, A. Stuck, P. Aebi, and L. Schlapbach, J. Electron Spectrosc. Relat. Phenom. **68**, 1 (1994).
[11] T. Greber and J. Osterwalder, Chem. Phys. Lett. **256**, 653 (1996).
[12] S. Y. Tong, H. Huang, and C. M. Wei, Phys. Rev B **46**, 2452 (1992).
[13] L. Floreano, G. Naletto, D. Cvetko, R. Gotter, M. Malvezzi, L. Marassi, A. Morgante, A. Santaniello, A. Verdini, F. Tommasini, and G. Tondello, Rev. Sci. Instrum. **70**, 3855 (1999). See http://tasc.area.trieste.it/tasc/lds/aloisa/aloisa.html
[14] A. Stuck, D. Naumović, H. A. Aebischer, T. Greber, J. Osterwalder, and L. Schlapbach, Surf. Sci. **264**, 380 (1992).